# Design of a Kinetic-Inductance Impedance-Matched Parametric Amplifier Using an Inverted Microstrip Architecture

Boon-Kok Tan[a*] and Peter K. Day[a,b]

[a]Dept. of Physics (Astrophysics), Univ. of Oxford, DWB Keble Road, OX1 3RH, Oxford, U.K.
[b]Jet Propulsion Laboratory (NASA), 4800 Oak Grove Dr., Pasadena 91109, CA, USA.

## ABSTRACT

Josephson-junction-based parametric amplifiers (JPAs) are key enabling technologies in superconducting quantum electronics, supporting applications ranging from dark-matter detection to quantum-computing readout. However, conventional JPAs are intrinsically narrowband, motivating the development of broadband architectures such as impedance-matched parametric amplifiers (IMPAs), which enhance bandwidth through the incorporation of auxiliary passive resonators.

In this work, we present the design and fabrication of a three-pole kinetic-inductance impedance-matched parametric amplifier (KIMPA) based on a niobium titanium nitride (NbTiN) nonlinear nanowire and implemented using an inverted microstrip architecture. The amplifier is synthesised using the multipole filter-design framework of Naaman and Aumentado and targets a 10% fractional bandwidth centred at 6 GHz with 20 dB gain. The device employs a multilayer architecture consisting of a 30 nm NbTiN wiring layer, a 150 nm amorphous-silicon dielectric layer, and a 200 nm niobium sky plane, enabling compact parallel-plate capacitors and improved fabrication robustness compared with conventional coplanar-waveguide implementations.

The design methodology is presented from the graph-based filter-synthesis model through circuit-level implementation and physical layout generation. Harmonic-balance simulations predict approximately 20 dB gain across a 6.0–6.4 GHz operating band, demonstrating the feasibility of broadband kinetic-inductance parametric amplification in an inverted microstrip platform. Fabricated devices have been completed and are currently being prepared for cryogenic characterisation.

**Keywords:** Impedance Match, Parametric Amplifier, Resonators, Niobium Titanium Nitride, Kinetic Inductance, Nanowire, Broadband, Inverted Microstrip, Harmonic Balance

## 1. INTRODUCTION

Josephson-junction-based parametric amplifiers (JPAs)[1] have become indispensable components in superconducting quantum electronics, enabling ultra-sensitive measurements in applications including dark matter searches,[2] neutrino mass determination experiments,[3] quantum-computing readout systems,[4,5] and many others. Conventional JPAs are inherently narrowband devices. To extend their tunable operating range, most implementations employ superconducting quantum interference devices (SQUIDs)[6,7] rather than individual Josephson junctions as the nonlinear inductive element, allowing the resonant gain frequency to be adjusted via magnetic flux applied to the SQUID loop.

Considerable effort has been devoted to increasing the bandwidth of JPAs. One of the most significant developments in this area is the travelling-wave parametric amplifier (TWPA),[8,9] which provides amplification bandwidths that are orders of magnitude larger than those of conventional resonant JPAs. However, TWPAs typically require either long nonlinear transmission lines or large arrays of Josephson junctions (or SQUIDs), increasing fabrication complexity and often reducing device yield.

An alternative approach to bandwidth enhancement is to couple one or more passive resonators to the nonlinear amplifier. Devices based on this principle are commonly referred to as impedance-matched parametric

*E-mail: boonkok.tan@physics.ox.ac.uk

amplifiers (IMPAs). This concept has been demonstrated in several implementations[10–13] and was rigorously formalised by Naaman and Aumentado,[14] who introduced a comprehensive filter-synthesis framework for broadband parametric amplifier design. Their methodology has since provided a unified basis for understanding and generalising IMPA architectures.

Most reported IMPAs employ SQUID-based nonlinear inductors or arrays of Josephson junctions, while only a limited number utilise highly nonlinear kinetic-inductance (KI) nanowires.[15] These kinetic-inductance impedance-matched parametric amplifiers (KIMPAs) have generally been limited to two-pole designs with bandwidths of approximately 6%. In this work, we apply the design methodology of Naaman and Aumentado[14] to realise a three-pole KIMPA with an anticipated bandwidth of approximately 10% centred at 6 GHz.

The amplifier is implemented using a niobium titanium nitride (NbTiN) thin film, a material previously demonstrated in KI-based TWPAs.[16] Replacing Josephson-junction-based nonlinear inductors with KI nanowires offers several advantages. First, the large superconducting gap of NbTiN extends the potential operating frequency range beyond that achievable with the aluminium tunnel junctions commonly used in JPAs and IMPAs. Although niobium-based junction technologies can similarly increase the operating frequency, their performance remains constrained by the intrinsic plasma resonance of the junction.

Second, whereas the nonlinear inductance of a Josephson junction is directly linked to its critical current ($I_c$), the nonlinear inductance of a KI nanowire can be engineered with greater flexibility through its geometry. In particular, the inductance can be adjusted through the nanowire aspect ratio while retaining independent control over ($I_*$), the characteristic current that determines the scale of nonlinear inductance modulation. KI nanowires are also substantially less sensitive to external magnetic fields and typically exhibit significantly higher 1 dB gain-compression point than junction-based parametric amplifiers.

A principal limitation of KI nanowires is that the achievable inductance modulation is typically restricted to approximately 15–20%, since the critical current of the nanowire is generally only about one-third of $I_*$. Nevertheless, operating junction-based IMPAs at similarly large fractions of $I_c$ is also challenging, as this can drive the system into higher-order nonlinear and potentially chaotic operating regimes that are not readily captured by existing analytical models.[17]

Most IMPAs and JPAs are implemented using single-layer coplanar-waveguide (CPW) architectures. Although highly successful, CPW structures are susceptible to fabrication defects such as shorts across the CPW gap. In contrast, the KIMPA presented here employs an inverted microstrip architecture, in which the signal and ground planes are separated by a dielectric layer, thereby reducing the likelihood of such failures. The grounded sky plane additionally protects the wiring layer from handling-related damage. Furthermore, the microstrip geometry enables the use of compact parallel-plate capacitors in place of large interdigital capacitors, improving both device compactness and fabrication yield.

In this paper, we present the design methodology of a kinetic-inductance impedance-matched parametric amplifier based on an inverted microstrip architecture. We first describe the graph-based filter-synthesis framework introduced by Naaman and Aumentado,[14] followed by the derivation of the circuit parameters and the physical implementation of the device layout. Finally, we present harmonic-balance simulations predicting the amplifier gain response.

## 2. DESIGN SYNTHESIS

In this work, we design a degenerate four-wave-mixing kinetic-inductance impedance-matched parametric amplifier (KIMPA) with a target fractional bandwidth ($\Delta\omega$) of 10% centred at approximately 6 GHz. The amplifier is based on a three-pole Chebyshev prototype synthesised for 20 dB gain with 0.5 dB passband ripple and serves as a proof-of-concept demonstration of a kinetic-inductance implementation of the conventionally Josephson-junction-based IMPA architecture.

### 2.1 Graph Model

The design procedure adopted in this work follows the synthesis methodology introduced by Naaman and Aumentado.[14] From Appendix E of Ref. ,[14] the prototype coefficients for a three-pole Chebyshev network are:

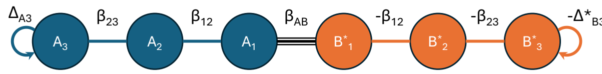


(a)

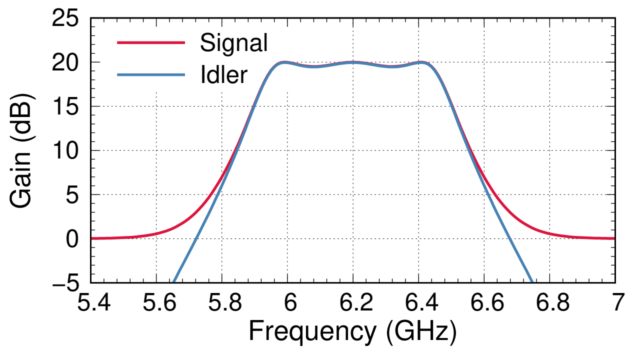


(b)

Figure 1. (a) Graph model depicting the signal and idler modes of a 3-pole network where the blue circles represent the signal path and the orange circles represents the idler circuit. (b) The calculated signal and idler gain based on the graph model.

$g_0$,...,$g_4$=1.0, 0.5899, 0.6681, 0.3753, 0.9045, where $g_0$ corresponds to the primary nonlinear resonator, comprising the kinetic-inductance nanowire and its associated shunt capacitance, which together define the centre frequency of the amplifier. The coefficient $g_4$ represents the external coupling to the input port.

Fig. 1 (a) shows the coupled-mode graph corresponding to the three-pole KIMPA design. Modes $A_x$ represent the signal network, while modes $B_x$ denote the conjugate idler network. Identical coupling coefficients are used for both signal and idler paths in our case. Here, we use the same coupling coefficients $\beta_x$ for both signal and idler circuit i.e.,

$$\beta_{12} = \frac{\Delta\omega}{(2\gamma_0\sqrt{g_1 g_2})} \quad \text{and} \quad \beta_{23} = \frac{\Delta\omega}{(2\gamma_0\sqrt{g_2 g_3})}. \tag{1}$$

where $\Delta\omega$ is the fractional bandwidth of the KIMPA, and $\gamma_0 = \gamma_{34} = \Delta\omega/(g_3 g_4)$. The signal and idler modes are coupled through the parametric interaction term $\beta_{AB} = \frac{g_3 g_4}{2 g_0 g_1}$, driven by a four-wave-mixing pump at frequency $\omega_P = \frac{1}{2}(\omega_A + \omega_B)$, where $\omega_A$ and $\omega_B$ are the centre frequencies of the signal and idler networks, respectively. For a degenerate IMPA, $\omega_A = \omega_B$.

The signal and idler gains are obtained from a $6 \times 6$ tridiagonal equation-of-motion matrix expressed in the modal basis $[A_3, A_2, A_1, B_1^*, B_2^*, B_3^*]$:

$$\mathbf{M} = \begin{bmatrix} \Delta_{A3} & \beta_{23} & 0 & 0 & 0 & 0 \\ \beta_{23} & \Delta_{A2} & \beta_{12} & 0 & 0 & 0 \\ 0 & \beta_{12} & \Delta_{A1} & \beta_{AB} & 0 & 0 \\ 0 & 0 & -\beta_{AB}^* & -\Delta_{B1}^* & -\beta_{12} & 0 \\ 0 & 0 & 0 & -\beta_{12} & -\Delta_{B2}^* & -\beta_{23}^* \\ 0 & 0 & 0 & 0 & -\beta_{23} & -\Delta_{B3}^* \end{bmatrix} \tag{2}$$

where $\Delta_{A1} = \Delta_{A2} = (1/\gamma_0)(\omega_s - \omega_A)$, $\Delta_{A3} = (1/\gamma_0)(\omega_s - \omega_A + i\gamma_{34}/2)$, $\Delta_{B1}^* = \Delta_{B2}^*(-1/\gamma_0)(\omega_s - 2\omega_p + \omega_B)$, and $\Delta_{B3}^* = (-1/\gamma_0)(\omega_s - 2\omega_p + \omega_B + i\gamma_{34}/2)$. Here, $\omega_s$ denotes the sweeping signal frequency.

The signal gain is obtained from the scattering parameter $S_{AA} = i\mathbf{M}_{AA} - 1$, while the idler gain is given by $S_{BA} = i\mathbf{M}_{BA}$, where $\mathbf{M}_{AA}$ and $\mathbf{M}_{BA}$ are the first and last elements of the inverse matrix $\mathbf{M}^{-1}$, respectively. The resulting signal and idler gain responses are shown in Fig. 1 (b). The model predicts approximately 20 dB of gain over the frequency range 6.0–6.4 GHz for $\omega_A = \omega_B = 6.2$ GHz and $\Delta\omega = 0.6$ GHz.

The design centre frequency was intentionally shifted from the target value of 6.0 GHz to 6.2 GHz. The filter-synthesis framework does not account for the pump-induced resonance-frequency shift that occurs during amplifier operation and is expected to move the gain profile towards lower frequencies. Consequently, the unpumped design is centred at a slightly higher frequency to compensate for this effect.

## 2.2 Circuit Model

The graph-based synthesis procedure described above does not directly specify the circuit-element values required to realise the three-pole IMPA. The circuit implementation depends on the chosen inverter architecture and the characteristic impedances of the ancillary resonators. However, all required component values can be readily extracted from the filter-synthesis model. In this work, we adopt the J-inverter implementation for the parametric couplings. An equivalent K-inverter formulation may also be used, and the corresponding derivation is provided in Ref.[14]

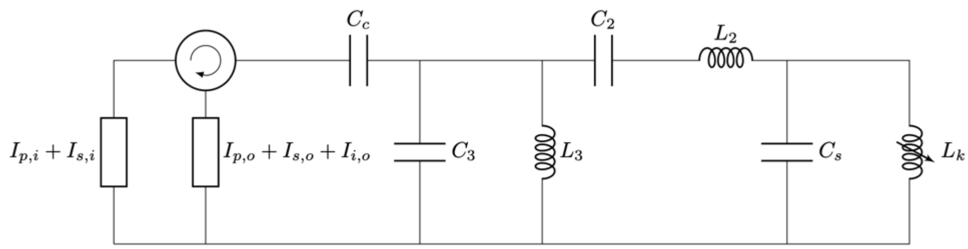


Figure 2. The circuit topology used in this manuscript to construct the 3-pole KIMPA comprising a parallel-series-parallel resonators configuration.

Fig. 2 shows the circuit topology selected for the three-pole KIMPA. The design employs a parallel–series–parallel resonator configuration. We begin by specifying the unpumped inductance of the nonlinear kinetic-inductance nanowire, which serves as the primary parametric mixing element of the amplifier. The nanowire inductance is chosen to be $L_{k0} = 200\,\text{pH}$, a value that can be conveniently realised using a $6\,\text{pH}/\square$ NbTiN film with an aspect ratio of approximately 30.

The shunt capacitance required to resonate the nonlinear resonator at the designated central frequency is given by $C_s = 1/(L_{k0}\omega_0^2)$, where $\omega_0 = \omega_A = \omega_B$ for the degenerate IMPA considered here. The embedding impedance of the nonlinear resonator is then $Z_{PA} = 1/\omega_0 C_s$ from which the reference impedance is obtained as $Z_{ref} = g_1 \frac{\omega_0}{\Delta\omega} Z_{PA}$.

Using $Z_{\text{ref}}$, the impedances of the second- and third-order passive resonators are calculated as $Z_2 = g_2 \frac{\omega_0}{\Delta\omega} Z_{ref}$ and $Z_3 = g_3 \frac{\omega_0}{\Delta\omega} Z_{ref}$. The corresponding inductance and capacitance values are then determined from the standard relations $C = \frac{1}{Z\omega_0}$ and $L = \frac{Z}{\omega_0}$. For the present design, this yields $C_s = 3.3\,\text{pF}$, $C_2 = 50.1\,\text{fF}$, $L_2 = 13.2\,\text{nH}$, $C_3 = 2.1\,\text{pF}$, and $L_3 = 314.4\,\text{pH}$.

To match the impedance $Z_3$ to a $Z_0 = 50\,\Omega$ environment, an additional J-inverter is introduced between the third resonator and the input port in the form of a coupling capacitor, $C_c = {}^{J_1}/_{\omega_0}({}^{1}/\sqrt{1 - Z_0^2 J_1^2})$. The introduction of $C_c$ modifies the effective capacitance of the third resonator. Consequently, the physical resonator capacitance must be adjusted according to $C_3 \to C_3 - C_3'$, where $C_3' = {}^{J_1}/_{\omega_0}\sqrt{1 - Z_0^2 J_1^2}$. This correction ensures that the resonator maintains the desired resonance frequency after the input matching network is incorporated.

# 3. HARMONIC BALANCE SIMULATION WITH CIRCUIT MODEL

With the preliminary circuit-element values determined from the filter-synthesis procedure, harmonic-balance simulations were performed using Keysight® Advanced Design System (ADS) to evaluate the gain–bandwidth performance of the KIMPA and further optimise the circuit parameters. This step is essential in the design of impedance-matched parametric amplifiers, as harmonic-balance analysis accounts for nonlinear wave-mixing processes, harmonic generation, and pump-induced variations in circuit parameters. Consequently, it provides a more realistic representation of amplifier behaviour than the linear synthesis framework alone.

| Components | Value | Unit | Width (µm) | Length (µm) |
|---|---|---|---|---|
| $L_{k0}$ | 172.6 | pH | 0.25 | 7.19 |
| $C_s$ | 3.29 | pF | 6.00 | 12.26 |
| $L_2$ | 13.15 | nH | N/A | N/A |
| $C_2$ | 50.11 | fF | 3.00 | 4.28 |
| $L_3$ | 314.36 | pH | 1.00 | 52.39 |
| $C_3$ | 1.97 | pF | 6.00 | 9.49 |
| $C_c$ | 1.2 | pF | 6.00 | 7.41 |

Table 1. Finalised values and dimension of the various inductors and capacitors components making up the amplifier. Note that the dimension of $C_2$ is presented as $2 \times C_2$ due to how this component shall be laid out topologically (see Fig. 4). The dimension of the spiral inductor $L_2$ is given in Table 2.

Although recent versions of ADS include dedicated models for Josephson-junction-based nonlinear devices, an equivalent component for highly nonlinear kinetic-inductance nanowires is not currently available. An alternative implementation is therefore required to exploit the harmonic-balance capabilities of ADS for the simulation of KI-based parametric amplifiers.

The nonlinear nanowire can be represented in ADS using either a Symbolically Defined Device (SDD) or a nonlinear inductor model. In this work, the latter approach is adopted, with the inductance defined as $L_{nl} = L_{k0}[1 + \beta_{nl}(\frac{I_p}{I^*})^2]$, where $L_{k0}$ is the unpumped kinetic inductance, $\beta_{nl}$ is the nonlinearity coefficient, $I_p$ is the pump-current amplitude, and $I^*$ is the nonlinear current scale parameter. For thin-film kinetic-inductance nanowires, $\beta_{nl} = 1$, whereas $\beta_{nl} = 0.5$ for Josephson-junction-based devices.[18,19] For the 250 nm wide and 30 nm thick NbTiN nanowire considered here, $I^*$ is expected to be of the order of 1 mA.

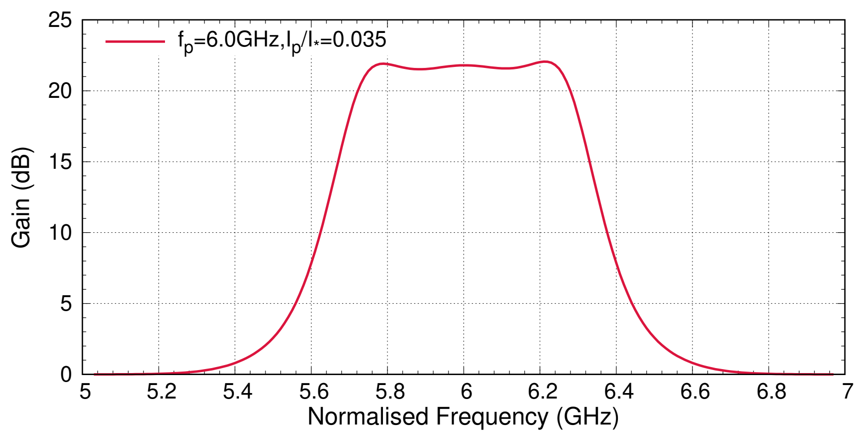


Figure 3. The signal gain profile predicted by ADS harmonic balanced model with the KIMPA pumped at 6 GHz with an amplitude of $I_p = 0.035I_*$.

The complete circuit shown in Fig. 2 was implemented in ADS, including an ideal circulator to separate the incident signal from the reflected amplified output. A $\mathrm{P_{nTone}}$ source was used to simultaneously inject the pump tone and the swept signal tone into the amplifier. Both tones were configured to include harmonic components up to the fifth order, while the harmonic-balance solver was set to a maximum mixing order of five. The circuit-element values obtained from the synthesis procedure were then refined to maximise the gain–bandwidth product of the amplifier. The resulting gain response is shown in Fig. 3.

The optimised component values are summarised in Table 1. Relative to the initial synthesis results, the most significant adjustment was made to the nanowire inductance ($L_{k0}$). This modification compensates for the pump-induced resonance-frequency shift that is not captured by the filter-synthesis framework, thereby ensuring that the gain profile remains centred at the target frequency of 6 GHz under operating conditions.

The final harmonic-balance simulation predicts a gain response centred at 6 GHz when pumped at the same frequency with a pump amplitude of $I_p = 0.035I^*$, as shown in Fig. 3. This operating point remaining comfortably below the commonly adopted design guideline of $I_p \lesssim 0.2 I_*$. Consequently, the amplifier is expected to operate well within the superconducting regime while providing sufficient nonlinear inductance modulation to achieve the desired parametric gain.

## 4. KIMPA LAYOUT WITH INVERTED MICROSTRIP TRANSMISSION LINE

Following optimisation of the circuit-element values, the final stage of the design process is the conversion of the circuit model into a physical device layout. For the present KIMPA, we adopt the inverted microstrip architecture previously demonstrated in kinetic-inductance travelling-wave parametric amplifiers (TWPAs).[16] As discussed in Sec. 1, this transmission-line architecture offers several advantages, including improved robustness against fabrication defects and a substantially reduced device footprint through the use of compact parallel-plate capacitors.

The device is implemented using a 30 nm thick niobium titanium nitride (NbTiN) wiring layer with an estimated unpumped sheet inductance of 6 pH/□. This layer is separated from a 200 nm thick niobium (Nb) sky plane by a 150 nm thick amorphous silicon (aSi) dielectric layer with relative permittivity $\epsilon_r = 10.3$. The complete structure is fabricated on a 675 µm thick silicon substrate.

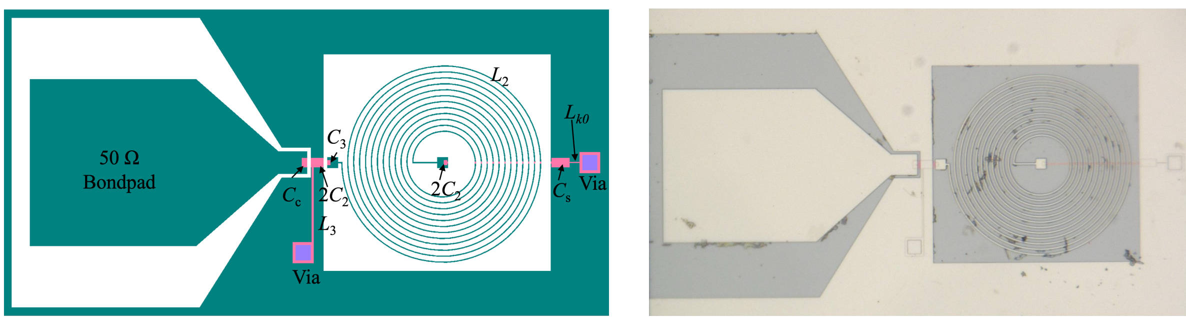


(a) (b)

Figure 4. (a) Layout of the 3-pole KIMPA where the pink areas are the NbTiN microstrip layer and the dark green areas represents the Nb sky plane. The purple squares are vias that connects the microstrip layer to the sky plane. The aSi layer is not clearly visible as it covers the entire area of the chip. (b) A microscope image of one of the fabricated device.

Fig. 4 (a) shows the final layout of the three-pole KIMPA. Once the layer stack and material properties are specified, the dimensions of the inductive and capacitive elements can be determined directly from the optimised circuit values. Because most circuit elements are implemented using the NbTiN wiring layer, care is taken to ensure that the passive resonators operate in a predominantly linear regime. This is achieved by using sufficiently wide conductors for the passive structures, thereby reducing current density and suppressing unwanted kinetic-inductance nonlinearity.

All capacitive elements are realised as parallel-plate capacitors, taking advantage of the multilayer inverted-microstrip geometry to minimise chip area. The capacitor dimensions are determined using the standard parallel-plate expression, $C = \epsilon_R \epsilon_0 A/d$, where $\epsilon_R$ is the dielectric constant of the aSi layer, $\epsilon_0$ is the vacuum permittivity, $A$ is the capacitor area, and $d$ is the dielectric thickness.

The inductors $L_{k0}$ and $L_3$ are implemented as high-aspect-ratio inverted-microstrip traces. Their inductances are determined primarily by the product of the conductor aspect ratio and the NbTiN sheet inductance. In the case of the passive resonator inductance $L_3$, the conductor width is intentionally increased to minimise residual nonlinear behaviour.

Implementing the large inductance $L_2$ using a straight microstrip trace would require an impractically long structure. Instead, the upper Nb sky plane is patterned to form a compact stripline spiral inductor. The dimensions of this spiral were estimated using the analytical expressions presented by Mohan et. al.,[20] with additional corrections to account for the inductance contribution of the underpass stripline connecting $C_s$ to the centre of the spiral. This underpass corresponds to the narrow NbTiN trace visible beneath the spiral structure

| $L_2$ | Value | Unit |
|---|---|---|
| No. of turns | 12 | turns |
| Turn spacing | 3 | µm |
| Turn width | 1.36 | µm |
| Outer diameter | 140.00 | µm |
| Inner diameter | 41.36 | µm |
| Under-bridge width | 1.00 | µm |
| Under-bridge length | 70.00 | µm |

Table 2. Dimensions of the spiral inductor $L_2$.

in Fig. 4 (a). The final dimensions of the complete set of component dimensions for the three-pole KIMPA is provided in Table 1 and the dimension of the spiral inductor are summarised in Table 2.

Fig. 4 (b) shows a microscope image of a fabricated device. Fabrication was carried out using the facilities of the Microdevices Laboratory (MDL) at the Jet Propulsion Laboratory (JPL). At the time of writing, the fabricated devices are undergoing packaging and integration into dedicated amplifier housings. Cryogenic measurements are planned to characterise the gain, bandwidth, and noise performance of the KIMPA and to compare the measured response with the predictions of the synthesis and harmonic-balance models.

## 5. CONCLUSION

We have presented the design and fabrication of a three-pole KIMPA based on an NbTiN nonlinear nanowire and implemented using an inverted microstrip architecture. The amplifier design follows the filter-synthesis framework developed by Naaman and Aumentado, beginning with a graph-based coupled-mode model and progressing through circuit-level synthesis, harmonic-balance optimisation, and physical layout implementation. The resulting design targets a 10% fractional bandwidth centred at 6 GHz with approximately 20 dB gain. Harmonic-balance simulations performed in Keysight ADS predict broadband amplification over the 6.0–6.4 GHz frequency range while accounting for the nonlinear behaviour of the kinetic-inductance nanowire and higher-order wave-mixing processes.

The inverted microstrip implementation enables the use of compact parallel-plate capacitors, reduces susceptibility to fabrication defects commonly encountered in coplanar-waveguide structures, and provides a practical route towards high-yield fabrication of broadband superconducting parametric amplifiers. The fabricated devices are currently being packaged for cryogenic characterisation. Future work will focus on measurements of gain, bandwidth, saturation power, and noise performance, as well as comparison of the measured results with the predictions of the synthesis and harmonic-balance models.

## ACKNOWLEDGMENTS

The authors would like to thank Ofer Naaman (Google Quantum AI) for advice in simulating the KIMPA in Keysight ADS, Dr. Rick LeDuc (MDL, JPL) for fabricating the device, and Florent Reix (LUX, Paris Observatory) for helping to dice the devices. Dr. P. Day is the Leverhulme Visiting Professor at the University of Oxford, funded by the Leverhulme Trust, when this work is being conducted. This research was funded in part by the European Commission's Horizon Europe Horizon-Infra-2022-Tech-01 programme RADIOBLOCKS (Project ID: 101093934), STFC Astronomy Observation and Theory Small Award (Project No. ST/Y002210/1), European Research Council (ERC) under the European Union's Horizon 2020 research and innovation programme with grant agreement No. [803862] (Project SPA4AstroQIT) and 101169947 (SPARTAN-FX), the MERAC Foundation and the STFC Quantum for Science Grant (ST/Y004973/1). For the purpose of Open Access, the author has applied a CC BY public copyright license to any Author Accepted Manuscript version arising from this submission. Views and opinions expressed are however those of the author(s) only and do not necessarily reflect those of the European Union or the European Research Council. Neither the European Union nor the granting authority can be held responsible for them.

## REFERENCES


[1] Aumentado, J., "Superconducting parametric amplifiers: The state of the art in josephson parametric amplifiers," *IEEE Microwave magazine* **21**(8), 45–59 (2020).

[2] Berlin, A. and Kahn, Y., "New technologies for axion and dark photon searches," *Annual Review of Nuclear and Particle Science* **75** (2025).

[3] Parno, D. S., "Overview of neutrino-mass determination," *arXiv preprint arXiv:2601.01672* (2026).

[4] Patel, P. S. and Desai, D. B., "Review of qubit-based quantum sensing," *Quantum Information Processing* **24**(3), 83 (2025).

[5] Yadlapati, M., "Quantum computing systems with qubit technology: A technical overview," *Journal of Computer Science and Technology Studies* **7**(2), 270–275 (2025).

[6] Ponselvan, D. Y. S., "Introduction to superconducting quantum interference device," in [*Advances in Bioelectromagnetism*], 27–41, Elsevier (2026).

[7] Zhou, Z., Zhang, H., Huang, R., He, F., Xu, D., Yan, X., and Li, L., "Advancements in research and current applications of quantum sensor: superconducting quantum interference device," *The European Physical Journal Special Topics* **234**(30), 9985–10013 (2026).

[8] Macklin, C., O'Brien, K., Hover, D., Ernst, C., Kornjača, L., Birenbaum, L. I., Oliver, W. D., and Siddiqi, I., "A near–quantum-limited josephson traveling-wave parametric amplifier," *Science* **350**(6258), 307–310 (2015).

[9] Ho Eom, B., Day, P. K., LeDuc, H. G., and Zmuidzinas, J., "A wideband, low-noise superconducting amplifier with high dynamic range," *Nature Physics* **8**(8), 623–627 (2012).

[10] Joshi, V., Hazra, S., Ding, A., Miano, A., Dai, W., Umasankar, G., Kottandavida, A., Liu, G., Frunzio, L., and Devoret, M., "Lumped-element broadband snail parametric amplifier with on-chip pump filter for multiplexed readout," *Physical Review Applied* **24**(4), 044003 (2025).

[11] Patel, L., Hawaldar, S., Panikkar, A., Shankar, A., and Suri, B., "Impedance-engineered josephson parametric amplifier with single-step lithography," *Applied Physics Letters* **127**(25) (2025).

[12] He, K., Yu, Q., Yang, L., He, Y., Liu, J., and Chen, W., "Graphical impedance-matching method for a superconducting parametric amplifier," *Physical Review Applied* **21**(3), 034055 (2024).

[13] Kaufman, R., White, T., Dykman, M. I., Iorio, A., Sterling, G., Hong, S., Opremcak, A., Bengtsson, A., Faoro, L., Bardin, J. C., et al., "Josephson parametric amplifier with chebyshev gain profile and high saturation," *Physical Review Applied* **20**(5), 054058 (2023).

[14] Naaman, O. and Aumentado, J., "Synthesis of parametrically coupled networks," *PRX Quantum* **3**(2), 020201 (2022).

[15] Hung, C.-C., Kutsuma, H., Chang, C. W. S., Van Loo, A. F., and Nakamura, Y., "Broadband kinetic inductance parametric amplifiers with impedance engineering," *Physical Review Applied* **24**(6), 064019 (2025).

[16] Faramarzi, F., Stephenson, R., Sypkens, S., Eom, B. H., LeDuc, H., and Day, P., "A 4–8 GHz kinetic inductance traveling-wave parametric amplifier using four-wave mixing with near quantum-limited noise performance," *APL Quantum* **1**(3) (2024).

[17] Montilla, J. N., Klimovich, N., Barbier, A., Driessen, E. F., and Tan, B.-K., "Parametric amplification in a Josephson junction array Fabry-Pérot cavity," *Physica Scripta* **100**(9), 095016 (2025).

[18] Montilla, J. N. and Tan, B.-K., "Extending the kinetic-inductance travelling wave parametric amplifiers coupled-mode framework to other symmetric nonlinear mediums with $\chi(3)$ nonlinearity," *Superconductor Science and Technology* **38**(7), 075008 (2025).

[19] Tan, B.-K., Boussaha, F., Chaumont, C., Longden, J., and Montilla, J. N., "Engineering the thin film characteristics for optimal performance of superconducting kinetic inductance amplifiers using a rigorous modelling technique," *Open Research Europe* **2**, 88 (2023).

[20] Mohan, S. S., del Mar Hershenson, M., Boyd, S. P., and Lee, T. H., "Simple accurate expressions for planar spiral inductances," *IEEE Journal of solid-state circuits* **34**(10), 1419–1424 (2002).